This is the Accepted Manuscript version of an article published by IOP Publishing Ltd in **Nanotechnology** on 5 Sept 2017. IOP Publishing Ltd is not responsible for any errors or omissions in this version of the manuscript or any version derived from it. **The Version of Record is available online at https://doi.org/10.1088/1361-6528/aa8013**

Role of Al doping in the filament disruption in HfO_2 resistance switches

Stefano Brivio[1,], Jacopo Frascaroli[1], Sabina Spiga[1,*]*

[1] Laboratorio MDM, IMM – CNR, via C. Olivetti 2, 20862, Agrate Brianza, Italy
[*] E-mail: stefano.brivio@mdm.imm.cnr.it, sabina.spiga@ mdm.imm.cnr.it

Keywords: RRAM, Memristor, HfO_2, Doping, Modeling, Random Telegraph Noise, Retention

Resistance switching devices, whose operation is driven by the formation (SET) and dissolution (RESET) of conductive paths shorting and disconnecting the two metal electrodes, have recently received a great attention and a deep general comprehension of their operation has been achieved. However, the link between switching characteristics and material properties is still quite weak. In particular, doping of the switching oxide layer has often been investigated only for looking at performance upgrade and rarely for a meticulous investigation of the switching mechanism.

In this paper, the impact of Al doping of HfO_2 devices on their switching operations, retention loss mechanisms and random telegraph noise traces is investigated. In addition, phenomenological modeling of the switching operation is performed for device employing both undoped and doped HfO_2. We demonstrate that Al doping influences the filament disruption process during the RESET operation and, in particular, it contributes in preventing an efficient restoration of the oxide with respect to undoped devices.

1. Introduction

In recent years, two terminal devices able to change their resistance upon electrical stimulation have been experiencing a renewed interested by a large community of researchers. Indeed, once studied only for non-volatile memory applications as resistance random access memories (RRAMs),[1,2] resistance switching (RS) devices, or memristive devices, are now under investigation for very diverse applications, like sensor devices[3] and elemental constituents of alternative computational schemes, like the stateful or the neuromorphic ones.[4–8]

The most mature technology of resistance switching devices is the one relying on the aggregation and dissolution of electrically active defects into and from filamentary regions within the oxide matrix sandwiched between the two electrodes.[1,2,9,10] For such particular class of RRAM devices, the general comprehension of the physics of the switching has achieved a high level of detail, especially for HfO_2-based devices.[11–14] In particular, oxygen vacancies (V_O) are ubiquitously recognized as the constituents of the conductive filament (CF) because they give rise, within the HfO_2 bandgap, either to localized electronic levels or to dispersed electronics bands when they are localized or accumulated, respectively. Formation and migration energies of V_O in different oxide lattice structures, dynamics of CF formation and dissolution have been successfully simulated.[12,13,15–17] On the other hand, only to a limited extent, the developed models are able to predict in a quantitative manner the switching properties of the devices when the involved materials are changed or modified, so that routes for switching optimization are often experimentally investigated.[18–20] In particular, doping is a smart solution to adjust some microscopic properties of a fixed material framework (i.e. HfO_2), which may facilitate the comprehension of the link with the macroscopic measurable quantities. In fact, doping has been widely investigated as a way to manage the V_O concentration, generation and migration, thus allowing tuning the resistance switching performances.[13,21,22]

For instance, Al doping in HfO_2 has been demonstrated, also by the same authors, to reduce variability and influence the memory retention.[19,23–25]

In the present work, Al doping in HfO_2-based RRAMs is investigated to get an insight on the filamentary switching mechanism of the devices. It is demonstrated that, while the filament formation process (SET process) is almost unaffected by the Al doping, the filament dissolution process (RESET process) and the defectivity of the resulting restored oxide are largely influenced by the presence of Al atoms. In particular, many aspects of the memory performances of the devices, such as the memory resistance window, the retention and the noise characteristics show clear qualitative differences in undoped and doped devices. All the experimental results, together with the results of a phenomenological model, support a picture in which immobile defects sites due to Al dopant prevent an efficient restoration of the oxide during filament dissolution with consequent modification of the retention characteristics and noise traces.

2. Methods

2.1 Materials and Devices

Samples characterized in this work have structures consisting of 40 nm TiN/5.7 nm HfO_2/50 nm Pt and 40 nm TiN/5.7 nm Al:HfO_2/50 nm Pt. Metals are grown by sputtering at room temperature. HfO_2 and 7% Al doped HfO_2 are grown by atomic layer deposition (ALD) at 300°C.[26] Further details of all the phases of the fabrication process can be found in [9,19,26,27]. Devices are obtained by pattering the 40×40 μm^2 wide top Pt electrodes by optical lithography and lift-off process.

Devices are tested in an electrical probe station with the Source Measuring Units (SMUs) of a Keysight B1500A semiconductor parameter analyzer. Voltages are applied to the top electrodes while the bottom TiN electrodes are always grounded. To initiate the RS operation, the devices need a forming with a negative current ramp up to -1 mA that creates the conductive filament shorting the metal electrodes. Current ramps for forming operations are

employed for reducing the current overshoot at the moment of switching in a more efficient way with respect to voltage ramps. On the other hand, it has been verified that voltage ramps are similarly effective thanks to a competition between filament formation and disruption processes at opposite interfaces as described in [27]. The RESET operation at positive voltage dissolves partially the conductive filament and leads to the high resistance state (HRS). The SET operation that re-instates the conductive filament and leads to the low resistance state (LRS) is operated at negative voltages with a current compliance of -1 mA applied by the SMU. Retention measurements of the HRS are carried out by exposing a pool of 20 different devices to temperatures of 85°C, 125°C and 150°C without the application of any bias. The value of the device resistance is monitored at time intervals logarithmically arranged at room temperature (23°C) by applying a voltage ramp up to 10 mV in order to avoid any device disturbance.
The random telegraph noise (RTN) of the devices is characterized by acquiring the current fluctuation over time as a small bias voltage is applied across the memory oxide in the HRS. After reset programming, small biases up to 500 mV are applied at the metal electrodes while sampling the current at constant time intervals of either 10 ms or 1 s for a total time up to 1000 s.

2.2 Modelling Formulation

Modeling is performed with a one dimensional filamentary model that assumes that the forming process instates a cylindrical CF shorting the two electrodes. The RESET process partially dissolves the CF by restoring an oxide gap in between two residual filament ends that remain in contact with the electrodes. The SET process is described as a lateral filament growth from an initial very thin conductive path instating within the gap. The two processes are described through migrating filament edges in the vertical and lateral directions for RESET and SET respectively according to the following rate equations:[28]

$$\frac{d\Delta}{dt} = A_{RESET} \cdot e^{-\frac{E_{RESET}}{k_B T}}, \qquad \frac{dr}{dt} = A_{SET} \cdot e^{-\frac{E_{SET}}{k_B T}} \tag{1}$$

where Δ is the length of the gap within the filament and r is the radius of the filament constriction in between the two filament ends remaining after RESET operation. $A_{RESET,SET}$ are pre-exponential factors; $E_{RESET,SET}$ are the activation energies, k_B is the Boltzmann's constant and T is the effective temperature inside the filament or gap regions. In the literature, some authors propose to model the SET process into two phases, i.e. the vertical growth of a thin conductive filament and a following filament lateral expansion.[29,30] On the other hand, it has been demonstrated that the general RRAM behavior can be correctly described only by the lateral filament growth,[28,31] as in the present manuscript. The same authors recently found that a second order device behavior related to a two-steps filament instating process can be evidenced in HfO_2-based devices in the particular case of stimulation with repetition of subthreshold spikes.[14,17]

The temperature in the filament or gap regions is evaluated through the steady state Fourier equation giving the equilibrium temperature profile arising from the Joule effect as a heat source and the dissipation along the vertical direction towards the electrodes kept at room temperature

$$k_{therm} \frac{d^2T}{dz^2} + J^2 \rho_{electr} = 0, \tag{2}$$

where k_{therm} is either the thermal conductivity of the filament k_{fil} or of the oxide k_{gap}; J is the current density and ρ_{electr} is either the electric resistivity of the filament ρ_{fil} or of the oxide ρ_{ox} of the gap. Some authors have recently pointed out that the temperature evolution may extend to quite large timescales,[32] which would require the use of the time-dependent version of the Fourier equation; however, only dedicated experiments or operations typical of neuromorphic computing show those effects. For what concerns the simulation carried out in this manuscript, it has been acknowledged that the steady state condition is generally reached

in tens of ps so that the temporal evolution of the temperature raise can be neglected for the sake of simplicity.[31]

To evaluate the Joule heating dissipation, the electric conduction in filament and gap regions must be modeled. In the resistance ranges investigated in the present manuscript, the electric conduction in the filament is considered metallic according to several experimental observations.[11,31] On the contrary, the resistivity of the oxide is considered to depend exponentially on the electric field F_{gap} applied to it:

$$\rho_{ox} = \rho_{ox,0} \cdot e^{-\gamma F_{gap}} \quad (3)$$

which corresponds to a simplification of a Poole-Frenkel conduction, where $\rho_{ox,0}$ is the oxide resistivity at zero field and γ is a fitting constant accounting for the non-linearity of the current against the applied voltage.[28] For the simulations, the terms related to the CF evolution, the conduction and the thermal models are solved self consistently through a Matlab routine.

3. Results

3.1. Resistance Switching Features

Figure 1a shows the forming operation performed on 20 undoped (blue) and 20 Al doped HfO_2 devices (red). The symbols stand for the average over the 20 measurements displayed as lines. As the current is increased during the measurements, the voltage increases correspondingly up to the voltage value (forming voltage) where a rapid voltage snap back to low voltage occurs, symptomatic of the resistance drop of the electroforming event. The resistance before forming is larger for doped than for undoped devices definitely beyond the device-to-device variability in agreement with some literature data.[16,18] This observation is consistent with the fact that Al doping prevents crystallization of the HfO_2 films during ALD growth at 300°C.[33,34] Indeed, undoped HfO_2 films tend to crystallize above a certain critical thickness of about 6 nm for the particular growth conditions adopted in the present work. On the contrary, with Al insertion, crystallization into a cubic/tetragonal structure is obtained only

with a post-growth annealing at high temperatures.[34] Though HfO_2 thickness in the present work is below the crystallization threshold, it can be expected that 5 nm undoped HfO_2 films already present nanocrystalline grains (not visible with laboratory XRD measurements) with some boundary defects that significantly contribute to the leakage current. On the contrary, the doped oxide can be considered amorphous down to the very atomic scale, thus offering few electronic defect states for leakage conduction.

Figure 1b shows the resistance switching (RS) operation over 200 cycles of undoped HfO_2 (blue) and Al:HfO_2 (red) devices. Every single measurement is shown in lines, while the average is shown in symbols according to the legend in figure 1a. The cumulative probability plots for resistance values of HRS and LRS extracted from those measurements are shown in figure 1c. For the same RESET stop voltage of 2 V, doped devices present a reduced average resistance window compared to the undoped devices as a result of an evident decrease of the resistance in the HRS, according to some literature data.[22,23] On the contrary, it has been reported that much higher doping concentrations (18-45%) than the present one increase the HRS resistance.[18] The RESET transitions, as reported in figure 1b, are qualitatively different in the two device typologies. In agreement with the picture of filament formation and disruption during RS cycles, the reduced resistance in doped samples has to be associated with a different CF disruption mechanism and/or a different microscopic configuration of the gap region in the two devices. In the following, retention and random telegraph noise (RTN) characteristics of the HRS are presented and discussed together with the modeling of the switching operation in order to give an insight of the microscopic nature of the restored oxide inside the filament gap. It is worth mentioning that from figure 1c one can appreciate that the employed doping level allows improving the uniformity in the tails of the HRS distribution, at the expenses of a worsening of the LRS distribution. Some works in the literature demonstrate that Al doping improves uniformity of both LRS and HRS, though the doping level is not specified or different from the one employed in the present work.[16,23,24,35]

3.2 High Resistance State retention

Figure 2a-b reports the retention characteristics at 85°C for times up to 10^6 s of undoped and doped devices, respectively. Thin lines correspond to all the recorded experimental data and the thick line is the average over those measurements. For reference, the average LRS levels is shown as thick dashed lines. As previously noticed, the two device typologies are characterized by different HRS values and they show two main mechanisms for retention loss: (i) gradual resistance lowering, evident for the undoped devices in figure 2a and (ii) sharp resistance drop ending up close to the LRS, as indicated by the data reported with line and symbols in figure 2a-b. The two mechanisms have been recognized by other groups without clearly identifying a correlation with the involved materials.[23,36,37] In a previous publication, the same authors already described the gradual resistance lowering as a thermally activated process for undoped and intermediately doped 4% Al:HfO_2 devices.[19] The second source of retention loss shows no clear dependence on the temperature as shown by the percentage of devices affected by such mechanism for both device typologies as a function of temperature in figure 2c. The same figure 2c evidences that the sharp resistance drop is much more significant in 7% Al doped devices, as it affects nearly half of them. Indeed, it has been demonstrated by the same authors that, in undoped devices, the main source of retention loss over the usual target survival time of 10 years is the thermal gradual lowering of the resistance. On the contrary, it has been found that, in the same period of time, almost 84% of the doped devices undergo sharp resistance drop, making this mechanism the main source of retention loss for doped devices.[19] Furthermore it is worth noticing that the HRS resistance of Al:HfO_2 devices can be increased and brought to the same value as for undoped HfO_2 devices by increasing the RESET stop voltage to about 3.5-4 V. The main retention loss mechanism of the Al:HfO_2 HRS obtained in this way remains the sharp resistance drop as reported in ref. [19]. This evidence demonstrates that the main mechanism of retention loss is driven by the doping effects rather than by the

HRS resistance level. A similar evolution from gradual resistance lowering to sharp drops with doping has been observed also by other groups.[23]

In terms of filamentary conduction model, the appearance of sharp resistance drops that rapidly revert the memory state to a low resistance state implies that a conduction path arises in the filament gap between two consecutive measurements. The fundamental difference in terms of retention behavior between devices with undoped HfO_2 and Al-doped HfO_2 is contextualized in the next session in the framework of a filamentary model.

It is worth mentioning that devices that experience sharp resistance drop can be reset back to the HRS and operate again several switching cycles (data not shown). Moreover, it has been found that devices that already experienced a resistance drop have a large probability of undergoing the same failure process and fall towards about the same end resistance as in the previous cases (please refer to figure S1 and Table S1 in the **Supplementary Data**). Such observation may indicate that a certain microscopic configuration of the filament gap tends to collapse to the same resistance value and/or the same filament configuration independently of its past history.

3.3 Random Telegraph Noise

When a small read voltage is applied to the devices after programming in the HRS, it is possible to notice a current fluctuation over time between two (or more) current levels. This current signal is often referred to as random telegraph noise (RTN). However, RTN refers to a purely electronic phenomenon, while in resistive switching memory cells also ionic transport phenomena can lead to current fluctuations.[38,39]

RTN is a well-known reliability issue of filamentary RRAM devices which affects their read margin in particular when low power performance, associated to high resistances, are pursued.[39–43] Compact models have been developed for the simulation of noise traces or noise amplitudes.[38,40] Such models assume that defect sites localized either in the dissolved filament

portion (gap) or close to the CF can trap and release electrons, which temporarily alter the conduction in HRS and LRS, respectively.[39,40] On the other hand, an assessment of the material dependent properties of RTN features is still lacking in the literature, both experimentally and theoretically. Indeed, the interpretation of RTN features in resistance switching devices requires complex computational efforts employing kinetic Monte Carlo simulations applied to the atomistic description of the interrupted filament. Such sophisticated simulation studies have been performed mainly on undoped binary HfO_2 RRAM devices.[39]

The RTN features of HfO_2 and Al:HfO_2 devices are reported in figure 3a-b, respectively. Figure 3a shows distinct current levels for HfO_2 devices, whereas in figure 3b the current evolves continuously in doped HfO_2 devices. The differences between RTN features of HfO_2 and Al:HfO_2 is evident also from the time-lag plots reported in figure 3c-d, in which the $(n+1)^{th}$ point is plotted as a function of the preceding n^{th} point, allowing to identify autocorrelated variables accumulating along the diagonal of the quadrant. This representation evidences for the undoped HfO_2 devices the presence of discrete current levels as separated accumulation clouds along the diagonal of the plot. On the contrary, for doped devices, it is not possible to distinguish more than only one broad current level. Along with time-lag plots, useful information can be identified in the power spectral density (PSD) of the acquired time series as reported in figure 3e-f. For undoped devices, two main trends can be distinguished in the analyzed frequency range. At high frequency, the $1/f$ trend prevails, while at low frequency the main PSD follows the $1/f^2$ slope. In doped devices, the PSD follows a single $1/f$ slope. In the classical RTN theory[44], the $1/f^2$ slope indicates few dominating traps, while the $1/f$ slope is the fingerprint of a large number of superposing traps with different characteristic time constants.[45] Therefore, the PSD supports the evidence that in undoped devices a small number of traps in the gap within the filament produces current jumps among discrete current levels. On the contrary, the number of traps in the gap region of the doped devices is so high that a continuum of levels is available allowing smooth current fluctuations over time.

The RTN noise comparison is reported here at a fixed RESET stop voltage of 2 V, which brings the two devices typologies to different HRS resistance. The comparison at fixed HRS resistance, obtained by raising the RESET stop voltage of doped devices, has been also carried out and confirms the abovementioned qualitative differences between undoped and doped devices. A summary of the RTN features of doped devices programmed to a resistance state comparable to the HRS of undoped ones is reported in the **Supplementary Data** (figure S2).

In summary, the different RTN feature observed in the two devices typologies provides an additional ingredient for the comprehensive description of the impact of doping in the RESET features of HfO_2 devices as discussed in the following section.

3.4 Phenomenological Modeling of RESET and SET

The operation of the devices is simulated through the model of filament formation and dissolution formalized in section 2.2. It is assumed that, after forming, a cylindrical CF is created, representative of a filamentary region where a high concentration of oxygen vacancies allows the dispersion of electronic bands within the HfO_2 gap. As discussed in section 3, the subsequent RESET process is described as the formation of an insulating gap within the CF with length Δ according to equation 1. The CF configuration obtained after a RESET simulation is taken as the starting point for the SET simulation, which is described as the lateral growth of a conductive filament with radius r according to equation 1 within the CF gap. It is, then, verified for self-consistency that the final configuration of the SET simulation corresponds to the one that was assumed as the initial condition for the RESET simulation.

The simulated RESET processes for HfO_2 and Al:HfO_2 and their comparison with experimental data are reported in figure 4. The simulated I-V curves (lines) are compared to the average experimental ones (symbols) in figure 4a and c for undoped (blue) and doped devices (red), respectively. The corresponding evolution of CF gap, Δ, as a function of the applied voltage is reported in figure 4b and d. In figure 4a and c, the current initially grows

proportionally to the applied voltage up to the points i, since the CF is nearly continuous from top to bottom electrodes. Points i correspond to a very small gap length $\Delta \approx 0.08$ nm and occur for about the same voltage value for undoped and doped devices. According to figure 4b and d, the gap length was set to a minimal value of $\Delta = \Delta_{ini} = 5 \cdot 10^{-3}$ nm and then it starts opening for voltages lower than those of points i. However, the gap contributes significantly to the current reduction only from points i on (see panels a and c of figure 4). Since resistance values and RESET voltages (those corresponding to points i) are nearly the same for undoped and doped HfO_2 devices, CF configuration and resistivity are set nearly equal in the simulations and give rise to the same current, gap and temperature behavior up to points i. Indeed, figure 4e represents the CF filament configuration at point i as the gray area extending from the left side corresponding to the bottom electrode to the right side corresponding to the top electrode. In the same figure 4e, the temperature profiles form bottom to top electrodes for both HfO_2 and Al:HfO_2 are shown (right axes) and they overlap according to the above considerations.

As the voltage is increased above the RESET voltage, the current undergoes a decrease passing through points ii, which corresponds to $\Delta \approx 2.4$ nm. Above the RESET voltage the experimental data for undoped and doped devices start differentiating. Indeed, points ii occurs for different voltage values for the two device typologies. The simulations differ due to the values of oxide resistivity $\rho_{ox,0}$ and parameter γ, 1 mΩm and 6 nm/V for HfO_2 and 0.1 mΩm and 3.5 nm/V for Al:HfO_2, as also reported in table S2 of the **Supplementary Data**. The different conductivity also results in a different filament heating as shown by the temperature profiles at points ii in figure 4f (right axes), which also reports the achieved filament configuration (left axis). As the voltage is further increased from points ii, the gap opening process slows down and Δ reaches values of 4.3 nm and 5.4 nm for HfO_2 and Al:HfO_2 devices, respectively. Interestingly, the largest gap, obtained for doped devices, corresponds to a lower HRS resistance than the one of the devices with undoped HfO_2.

The simulated SET process is described in figure 5 for both HfO_2 and doped Al:HfO_2 devices. The simulated I-V curves (lines) are compared to the average experimental ones (symbols) in figure 5a and c for undoped (blue) and doped (red) devices, respectively. The corresponding evolution of CF radius, r, as a function of the applied voltage is reported in figure 5b and d.

The SET simulation starts form the HRS in which the CF dimension is negligible ($r = r_{ini} = 10^{-6}$ nm) and slowly increases for low voltages (between -0.4 and point i and between -0.5 V and point i for undoped and doped devices, respectively). In this regime and until points i are reached (figure 5a and c), the current does not deviate from the exponential growth accounting for the field-dependent oxide conductivity described above (equation 3). At points i, the temperature values are slightly different for undoped and doped devices as visible from the straight and dashed CF profiles and from the straight and dashed lines in figure 5e. However, the points i are where the SET process is considered to actually initiate for both device typologies since the current increases rapidly (figure 5a and c) and the CF radius change is almost vertical (figure 5b and d, see supplementary data for details). The configuration of the CF at point i is represented by the gray region in figure 5e (left axis), in which the CF in the constriction is subnanometric in size ($r \approx 0.1$ nm for both device typologies) but the temperature is high enough to promote the migration of oxygen vacancies and CF growth. From figure 5e, it is evident that the initial CF configurations of undoped (continuous line) and doped (dashed line) devices differ in the initial gap length, according to the results of the RESET simulation. The temperature profiles along the CF axis are reported in figure 5e for both undoped and doped HfO_2 devices, respectively (right axis). As the voltage is further increased, the CF radius grows according to figure 5b and d passing through points ii, whose corresponding CF configurations are shown in figure 5f. The final CF radii are very similar, i.e. 5.3 nm and 5.4 nm for undoped and doped HfO_2 devices, respectively.

In summary, the phenomenological simulations show that the different RESET characteristics of HfO_2 and Al:HfO_2 devices can be mainly ascribed to the different conduction properties of the restored oxide within the filament gap. In particular, the oxide of the gap in Al-doped device is more conductive than the one of the undoped oxide devices. Furthermore, the gap length is slightly larger for Al:HfO_2 than for HfO_2 devices despite the HRS resistance of the former is lower than the one of the latter. It must be reminded, though, that the phenomenological model gives only an average description of the measured I-V curves and the microscopic configuration of the CF during RESET can be quite different form the macroscopic picture of a gap within a CF as discussed in the following paragraph. Moreover, the parameter values have to be considered as effective values of the modeled processes. Hence, considering that the electroforming process provokes damages in the insulating layer of a RRAM device, which can only be partially recovered by a RESET operation, it can be concluded that, in undoped HfO_2 devices, the oxide insulating properties in the gap region can be restored to a larger extent with respect to the Al:HfO_2 devices, for the same applied RESET stop voltage. It must be emphasized that actually the pristine resistance is even larger for doped than for undoped oxide devices.

4. Discussion

In the previous sections, the experimental and the modeling investigations of TiN/HfO_2/Pt and TiN/Al:HfO_2/Pt devices have been presented. We summarize here the main observations. First of all, the doped oxide shows a higher initial resistance than the undoped oxide as shown in figure 1a. On the contrary, HRS is more insulating for the undoped devices rather than for the doped ones, as visible from figure 1b and c. These observations are in agreement with other results in the literature.[16,18,35] According to the filamentary model, the oxide of the gap is more conductive for the Al-doped case than for the undoped oxide case (table S2 in the **Supplementary Data**). Therefore, it can be concluded that the pristine doped

oxide is more insulating than the undoped oxide, whereas, after formation and dissolution of the CF, the doped oxide recovers an insulating state that is more conductive than the one of the undoped oxide.

Beyond the macroscopic difference in conductivity, retention and RTN features show that also at the microscopic scale the oxide of the gap has a different nature in undoped and doped devices. Indeed, the main retention loss mechanisms consist in a gradual resistance lowering for HfO_2 devices and in abrupt resistance drops for Al:HfO_2 devices, as discussed with reference to figure 2. Furthermore, HfO_2-based devices show a step-like RTN noise with a significant $1/f^2$ contribution, whereas Al:HfO_2-based devices show smooth resistance fluctuations in association with $1/f$ type of noise. It must be pointed out that experimental characterizations of devices with 4% Al doped HfO_2 have been performed and reveal the same features as undoped devices to a first approximation. A slight deviation is visible in the retention characteristics between undoped and 4% doped device as reported in [19]. Moreover, current-voltage curves of 4% doped device superimpose to those of undoped devices and, hence, both experimental data can be simulated with the same phenomenological modeling parameters. For these reasons, the 7% doping can be considered as the threshold concentration that determines a drastic change in the device characteristics.

In the following, we propose a qualitative picture that explains all these observations in a consistent fashion. It must be noticed that HfO_2 doping produces many interrelated consequences, as structural lattice adjustments,[26,46] variation of the energies of formation of the different kinds of oxygen vacancies close to doping sites,[21] modification of the mobility of oxygen vacancies,[13,16,47], all of which affect the physics of the resistance switching operation.

First of all, it must be reminded that undoped and Al doped HfO_2 present different structural properties. HfO_2 films grown by ALD completely crystallize in the monoclinic structure at relatively low temperatures (400-500°C)[26,46] and a polycrystalline structure can be resolved by XRD in as-deposited sample for thicknesses above 5-6 nm.[26,34] On the other hand,

nanocrystallites can be expected to form even at lower thicknesses and to present defects at their boundaries that promote the electrical conduction. On the contrary, such nanograins are absent in doped HfO_2 films that tend to crystallize in the cubic/tetragonal phase at much higher temperatures for similar thicknesses.[26,34] As a consequence, ALD grown doped films are usually more insulating than undoped ones.[16,18] On the other hand, comparable resistivities of undoped and doped oxides, or even reduced with doping, can be obtained in case amorphous structure is forced as in low temperature physical vapor deposition techniques.[22,35] Beyond these considerations, as stated above, the oxide of the gap, which determines the properties of the HRS, presents very different microscopic configurations in undoped and doped devices. The switching mechanisms of oxide filamentary devices rely on formation, migration and aggregation of defects, mainly oxygen vacancies V_O. All these processes are interconnected among each other and are largely affected by structural and electronics properties on the oxide hosting matrix.

For what concerns V_O creation, it is usually expected that doping with substitutional trivalent ions, like Al, favors V_O formation that compensates the electron deficiency.[46] Indeed, ab-initio calculations by different research groups evidence the fact that the energy of formation of oxygen vacancies is lower in proximity of a dopant ion than in a undoped stoichiometric oxide matrix.[13,16,22,48] On the other hand, also grain boundaries in polycrystalline structures are additional preferential locations for V_O formation.[11,49]

However, the V_O formation energy is not the only term influencing the device switching. The mobility of ionic Hf^{q+} and O^{q-} species has to be taken into account, as well, and it has been shown to depend both on the structure of the oxide matrix in which they are immersed[50] and on the proximity of a migration path to impurities. For instance, Schie et al.[51] have recently demonstrated the sub-diffusive nature of ion migration in amorphous HfO_2 compared to the standard energy activated migration in the crystalline phase. Correspondingly, also Vandelli et

al.[49] showed that the presence of grain boundaries, modeled as amorphous regions between two tilted crystalline regions, favors oxygen, or equivalently V_O, migration.

As cited above, the proximity to impurities or doping elements affects the migration barriers of ionic species in a complicated way, so that many theoretical works dedicated to such aspect.[13,15,16,21,52,53] For instance, Song et al.[47] have recently demonstrated that ion migration are largely affected by doping in such a way that V_O are attracted and remain stuck close to Al doping ions.

From an experimental point of view, the thermally activated HRS retention loss evidenced a decrease of the activation energy for resistance lowering from 1.5 eV to about 1.1. eV for undoped and 4% Al-doped HfO_2-based devices, which can be associated to a facilitation of diffusion processes of V_O and oxygen ions upon doping.[19]

On the other hand, as shown in figure 1a and b, forming and set voltages assume about the same value in undoped and doped devices, which indicates that the filament instating process, driven by both V_O formation and gathering through migration, follows nearly the same energetics. This conclusion is supported also by the use of the same effective activation energy for filament growth for the simulation of both device typologies.

In summary, a clear understanding of the impact of doping on all the interrelated factors influencing the switching mechanism is hard to be drawn from the existing literature. For this reason, we propose an interpretation which agrees with all the experimental results reported in the paper, in order to help addressing a more quantitative investigation of the topic.

Figure 6 shows a schematic view of the proposed CF configurations in LRS and HRS for both device typologies to support the discussion. The LRS is described as an accumulation of V_O in a filamentary path that connects top and bottom electrodes. In undoped HfO_2 films, V_O formation preferentially occurs in proximity of localized defects, e.g. at the boundaries of nanometric crystalline grains (not shown in figure 6). On the contrary, in Al:HfO_2, where seed crystalline clusters are expected to be absent, V_O formation is favored in proximity of the dopant

sites (dashed circles in figure 6), according to the above considerations. In the HRS, part of the CF is dissolved and, to some extent, the oxide is restored, opening a gap within the filament. It is expected that the oxide of the gap, though, still preserves some defectivity that is reminiscent of the previous presence of the conductive filament, which is depicted in figure 6 as a region defined by green dashed lines in the HRS. Such non-recovered defectivity configuration constitutes a preferential path for the diffusion of V_O, which lead to a gradual resistance lowering as seen in retention experiment on HfO_2 devices (figure 2a). In Al:HfO_2 samples, besides the non-recovered defectivity, the oxide of the gap is also affected by the presence of doping sites, which can be considered immobile as a first approximation.

It must be noticed that 7% Al doping corresponds to a very high doping density: e.g. assuming a tetragonal crystal structure (5 Hf atoms per cell), uniform substitutional doping without any tendency to Al accumulation, one Al ion is present every 3 unit cells, meaning that on average one cell containing one Al ion has at least one nearest neighboring cell with another Al ion. This crude estimation gives an average Al-Al distance of 0.5 nm (roughly the tetragonal cell dimension).[46]

As a consequence, the HRS of Al-doped devices can be characterized by the persistence in the gap region of V_O bound to immobile doping sites that contribute to the lowering of the oxide resistivity and HRS resistance despite the gap region can be described microscopically by the same effective dimension, in agreement with the simulations presented in figure 4. Furthermore, the high concentration of Al ions, i.e. V_O accumulation sites in the gap region, can be responsible for the fast spontaneous reassembly of the CF, leading to the abrupt resistance drop, which has been recognized as the main mechanism of retention loss in Al-doped devices, according to figure 2b and other reports in the literature.[19,23]

Furthermore, it has been noticed that devices that are re-cycled and reprogrammed after an abrupt resistance drop tend to experience abrupt drops and fall to about the same resistance values (see figure S1 and table S1 in the **Supplementary Data**). Also this fact is in agreement

with the presence of fixed sites of V_O accumulation that, with time, lead to the reassembly of CFs with similar microscopic configurations and similar overall device resistance.

The sketch reported in figure 6 is consistent also with the RTN features discussed with reference to figure 3 (see also figure S2 of the **Supplementary Data**), because the density of available sites for energetically favored V_O hosting largely increases with Al doping. Indeed, V_O sites have been identified as charge trapping and de-trapping centers responsible for resistance changes over time as those shown in figure 3.

5. Conclusions

In summary, undoped and 7% Al doped HfO_2 RRAM devices are investigated in their DC operation, retention and RTN characteristics and through modeling. First of all, it has been reported that doping increases the initial resistance of the devices, while decreases the HRS resistance for the same applied RESET stop voltage. Phenomenological modeling reveals that the resistance difference can be ascribed to different conduction properties of the restored oxide within the CF gap for devices with undoped and doped oxides.

Doping is also responsible for the retention loss mechanism due to abrupt resistance drop from HRS to LRS, which prevails over the thermal activated gradual lowering of HRS typical of undoped HfO_2 devices. Furthermore, the step-like RTN noise traces of HfO_2 devices has been shown to evolve to a continuous noise trace in Al:HfO_2, due to an increased number of superimposing contributions from electrically active defects. Such manifold investigation allows elaborating a comprehensive overview of formation and dissolution of CF responsible for the resistance switching as a function of doping. In particular, doping introduces immobile defect sites in the CF gap that are not present in the undoped devices, which prevent an efficient restoration of the oxide after filament formation and affect the conduction properties, the retention loss mechanisms and RTN features of the devices.

Acknowledgements

The work is partially supported by the European project H2020-ICT-2015 NEUral computing aRchitectures in Advanced Monolithic 3D-VLSI nanotechnologies (NEURAM3, grant agreement n. 687299). The authors acknowledge Dr. E. Cianci for the support on the oxide material synthesis and M. Alia for the support in the fabrication processes.

References

[1] D. S. Jeong, R. Thomas, R. S. Katiyar, J. F. Scott, H. Kohlstedt, A. Petraru, C. S. Hwang, *Rep. Prog. Phys.* **2012**, *75*, 076502.

[2] H.-Y. Chen, S. Brivio, C.-C. Chang, J. Frascaroli, T.-H. Hou, B. Hudec, M. Liu, H. Lv, G. Molas, J. Sohn, S. Spiga, V. M. Teja, E. Vianello, H.-S. P. Wong, *J. Electroceramics* **2017**.

[3] I. Gupta, A. Serb, A. Khiat, R. Zeitler, S. Vassanelli, T. Prodromakis, *Nat. Commun.* **2016**, *7*, 12805.

[4] J. Borghetti, G. S. Snider, P. J. Kuekes, J. J. Yang, D. R. Stewart, R. S. Williams, *Nature* **2010**, *464*, 873.

[5] R. Rosezin, E. Linn, C. Kugeler, R. Bruchhaus, R. Waser, *IEEE Electron Device Lett.* **2011**, *32*, 710.

[6] E. Covi, S. Brivio, M. Fanciulli, S. Spiga, *Microelectron. Eng.* **2015**, *147*, 41.

[7] D. Kuzum, S. Yu, H.-S. Philip Wong, *Nanotechnology* **2013**, *24*, 382001.

[8] E. Covi, S. Brivio, A. Serb, T. Prodromakis, M. Fanciulli, S. Spiga, *Front Neurosci* **2016**, *10*, 482.

[9] S. Brivio, G. Tallarida, E. Cianci, S. Spiga, *Nanotechnology* **2014**, *25*, 385705.

[10] J. Frascaroli, S. Brivio, F. Ferrarese Lupi, G. Seguini, L. Boarino, M. Perego, S. Spiga, *ACS Nano* **2015**, *9*, 2518.

[11] G. Bersuker, D. C. Gilmer, D. Veksler, P. Kirsch, L. Vandelli, A. Padovani, L. Larcher, K. McKenna, A. Shluger, V. Iglesias, M. Porti, M. Nafría, *J. Appl. Phys.* **2011**, *110*, 124518.

[12] A. Padovani, L. Larcher, O. Pirrotta, L. Vandelli, G. Bersuker, *IEEE Trans. Electron Devices* **2015**, *62*, 1998.

[13] B. Magyari-Köpe, L. Zhao, Y. Nishi, K. Kamiya, M. Y. Yang, K. Shiraishi, In *2014 IEEE International Symposium on Circuits and Systems (ISCAS)*; 2014; pp. 2021–2024.

[14] S. Brivio, E. Covi, A. Serb, T. Prodromakis, M. Fanciulli, S. Spiga, *Appl. Phys. Lett.* **2016**, *109*, 133504.

[15] S. Clima, B. Govoreanu, M. Jurczak, G. Pourtois, *Microelectron. Eng.* **2014**, *120*, 13.

[16] B. Traore, P. Blaise, E. Vianello, H. Grampeix, A. Bonnevialle, E. Jalaguier, G. Molas, S. Jeannot, L. Perniola, B. DeSalvo, Y. Nishi, In *Electron Devices Meeting (IEDM), 2014 IEEE International*; 2014; p. 21.5.1-21.5.4.

[17] S. Brivio, E. Covi, A. Serb, T. Prodromakis, M. Fanciulli, S. Spiga, In *Memristive Systems (MEMRISYS) 2015 International Conference on*; 2015; pp. 1–2.

[18] A. Fantini, L. Goux, S. Clima, R. Degraeve, A. Redolfi, C. Adelmann, G. Polimeni, Y. Y. Chen, M. Komura, A. Belmonte, others, In *Memory Workshop (IMW), 2014 IEEE 6th International*; IEEE, 2014; pp. 1–4.

[19] J. Frascaroli, F. G. Volpe, S. Brivio, S. Spiga, *Microelectron. Eng.* **2015**, *147*, 104.

[20] G. Molas, E. Vianello, F. Dahmani, M. Barci, P. Blaise, J. Guy, A. Toffoli, M. Bernard, A. Roule, F. Pierre, C. Licitra, B. De Salvo, L. Perniola, In *Electron Devices Meeting (IEDM), 2014 IEEE International*; 2014; p. 6.1.1-6.1.4.
[21] H. Zhang, B. Gao, S. Yu, L. Lai, L. Zeng, B. Sun, L. Liu, X. Liu, J. Lu, R. Han, others, In *Simulation of Semiconductor Processes and Devices, 2009. SISPAD'09. International Conference on*; IEEE, 2009; pp. 1–4.
[22] L. Zhao, S. W. Ryu, A. Hazeghi, D. Duncan, B. Magyari-Köpe, Y. Nishi, In *2013 Symposium on VLSI Technology (VLSIT)*; 2013; pp. T106–T107.
[23] C.-S. Peng, W.-Y. Chang, Y.-H. Lee, M.-H. Lin, F. Chen, M.-J. Tsai, *Electrochem. Solid-State Lett.* **2012**, *15*, H88.
[24] B. Gao, H. W. Zhang, S. Yu, B. Sun, L. F. Liu, X. Y. Liu, Y. Wang, R. Q. Han, J. F. Kang, B. Yu, Y. Y. Wang, In *2009 Symposium on VLSI Technology*; 2009; pp. 30–31.
[25] L. Chen, Y. Xu, Q. Q. Sun, P. Zhou, P. F. Wang, S. J. Ding, D. W. Zhang, *IEEE Electron Device Lett.* **2010**, *31*, 1296.
[26] E. Cianci, A. Molle, A. Lamperti, C. Wiemer, S. Spiga, M. Fanciulli, *ACS Appl. Mater. Interfaces* **2014**, *6*, 3455.
[27] S. Brivio, J. Frascaroli, S. Spiga, *Appl. Phys. Lett.* **2015**, *107*, 023504.
[28] S. Ambrogio, S. Balatti, D. C. Gilmer, D. Ielmini, *IEEE Trans. Electron Devices* **2014**, *61*, 2378.
[29] P. Huang, X. Y. Liu, B. Chen, H. T. Li, Y. J. Wang, Y. X. Deng, K. L. Wei, L. Zeng, B. Gao, G. Du, X. Zhang, J. F. Kang, *IEEE Trans. Electron Devices* **2013**, *60*, 4090.
[30] H. Li, P. Huang, B. Gao, B. Chen, X. Liu, J. Kang, *IEEE Electron Device Lett.* **2014**, *35*, 211.
[31] D. Ielmini, *IEEE Trans. Electron Devices* **2011**, *58*, 4309.
[32] S. Kim, C. Du, P. Sheridan, W. Ma, S. Choi, W. D. Lu, *Nano Lett.* **2015**, *15*, 2203.
[33] S. Spiga, F. Driussi, A. Lamperti, G. Congedo, O. Salicio, *Appl. Phys. Express* **2012**, *5*, 021102.
[34] G. Congedo, C. Wiemer, A. Lamperti, E. Cianci, A. Molle, F. G. Volpe, S. Spiga, *Thin Solid Films* **2013**, *533*, 9.
[35] S. Yu, B. Gao, H. Dai, B. Sun, L. Liu, X. Liu, R. Han, J. Kang, B. Yu, *Electrochem. Solid-State Lett.* **2010**, *13*, H36.
[36] B. Gao, H. Zhang, B. Chen, L. Liu, X. Liu, R. Han, J. Kang, Z. Fang, H. Yu, B. Yu, D. L. Kwong, *IEEE Electron Device Lett.* **2011**, *32*, 276.
[37] L. Zhang, R. Huang, Y. Y. Hsu, F. T. Chen, H. Y. Lee, Y. S. Chen, W. S. Chen, P. Y. Gu, W. H. Liu, S. M. Wang, C. H. Tsai, M. J. Tsai, P. S. Chen, In *Reliability Physics Symposium (IRPS), 2011 IEEE International*; 2011; p. MY.8.1-MY.8.5.
[38] F. M. Puglisi, P. Pavan, L. Vandelli, A. Padovani, M. Bertocchi, L. Larcher, In *Reliability Physics Symposium (IRPS), 2015 IEEE International*; 2015; p. 5B.5.1-5B.5.6.
[39] F. M. Puglisi, P. Pavan, L. Larcher, In *2016 IEEE International Reliability Physics Symposium (IRPS)*; 2016; p. MY-8-1-MY-8-5.
[40] S. Ambrogio, S. Balatti, A. Cubeta, A. Calderoni, N. Ramaswamy, D. Ielmini, In *Electron Devices Meeting (IEDM), 2013 IEEE International*; 2013; p. 31.5.1-31.5.4.
[41] N. Raghavan, R. Degraeve, A. Fantini, L. Goux, D. J. Wouters, G. Groeseneken, M. Jurczak, In *Electron Devices Meeting (IEDM), 2013 IEEE International*; 2013; p. 21.1.1-21.1.4.
[42] B. Guan, J. Li, In *2016 IEEE International Reliability Physics Symposium (IRPS)*; 2016; p. MY-5-1-MY-5-4.
[43] S. Choi, Y. Yang, W. Lu, *Nanoscale* **2014**, *6*, 400.
[44] W. Shockley, W. T. Read, *Phys. Rev.* **1952**, *87*, 835.
[45] M. B. Weissman, *Rev. Mod. Phys.* **1988**, *60*, 537.
[46] C.-K. Lee, E. Cho, H.-S. Lee, C. Hwang, S. Han, *Phys. Rev. B* **2008**, *78*.
[47] Y. Song, B. Magyari-Kope, Y. Lin, Y. Nishi, In *2017 IEEE International Memory Workshop (IMW)*; 2017; pp. 1–4.

[48] L. Zhao, S. Clima, B. Magyari-Köpe, M. Jurczak, Y. Nishi, *Appl. Phys. Lett.* **2015**, *107*, 013504.
[49] L. Vandelli, A. Padovani, L. Larcher, G. Broglia, G. Ori, M. Montorsi, G. Bersuker, P. Pavan, In *Electron Devices Meeting (IEDM), 2011 IEEE International*; IEEE, 2011; pp. 17–5.
[50] G. Broglia, G. Ori, L. Larcher, M. Montorsi, *Model. Simul. Mater. Sci. Eng.* **2014**, *22*, 065006.
[51] M. Schie, M. P. Müller, M. Salinga, R. Waser, R. A. De Souza, *J. Chem. Phys.* **2017**, *146*, 094508.
[52] S. Clima, Y. Y. Chen, A. Fantini, L. Goux, R. Degraeve, B. Govoreanu, G. Pourtois, M. Jurczak, *IEEE Electron Device Lett.* **2015**, *36*, 769.
[53] S. Clima, Y. Y. Chen, R. Degraeve, M. Mees, K. Sankaran, B. Govoreanu, M. Jurczak, S. D. Gendt, G. Pourtois, *Appl. Phys. Lett.* **2012**, *100*, 133102.

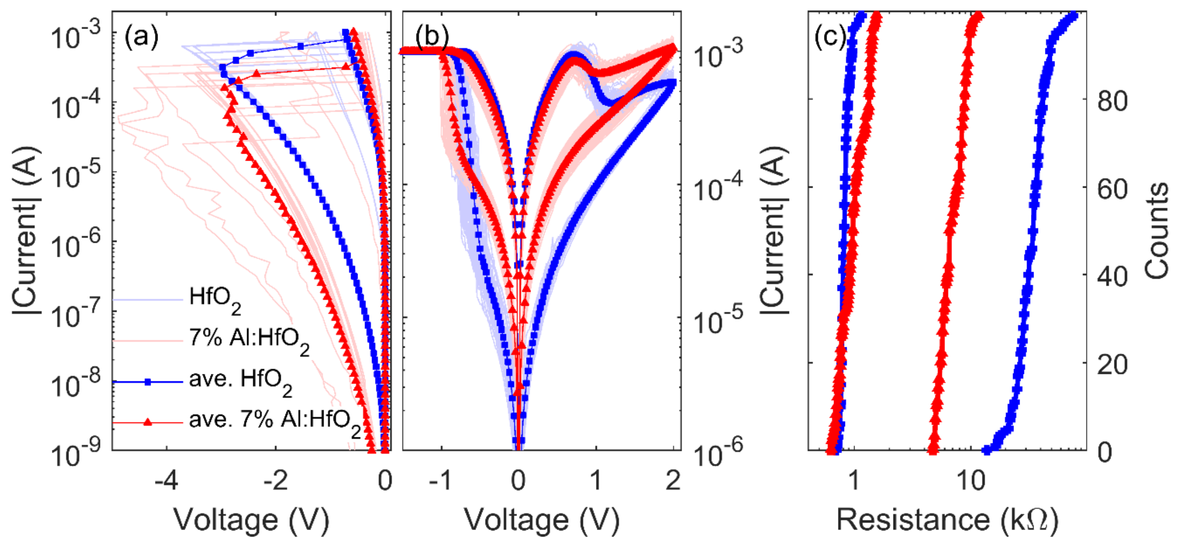

Figure 1. (a) Initialization of 20 fresh devices with forming at negative voltages. (b) RS curves with SET and RESET for negative and positive voltages, respectively. In lines 200 I-V curves on single devices and in symbols average curves for the two device typologies. (c) Cumulative probability plots of the resistances in HRS and LRS for both device typologies. Blue squares are for pure HfO_2 and red triangles for $Al:HfO_2$ according to the legend in panel (a).

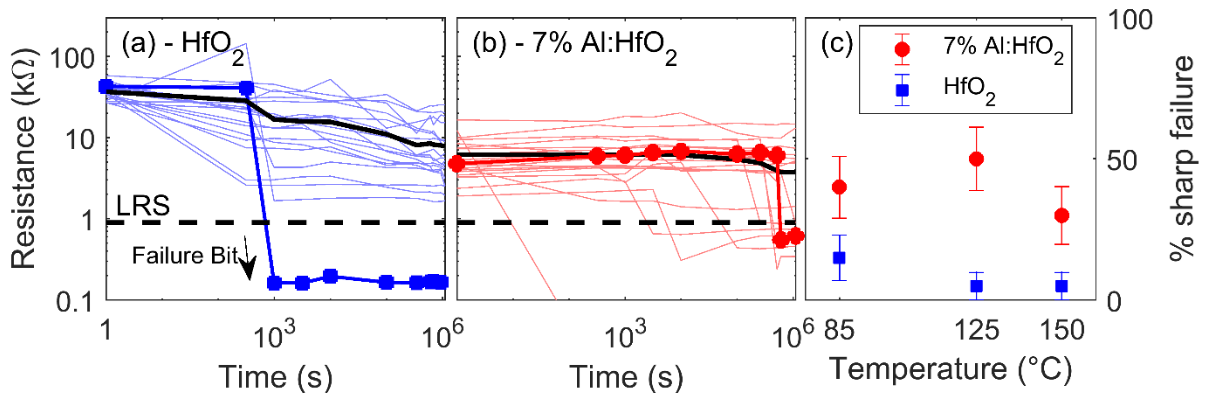

Figure 2. HRS state retention characteristics of 20 HfO_2 (a) and 20 7% $Al:HfO_2$ (b) devices obtained at 85°C (lines). The average HRS trend is indicated by the thick line. Representative sharp resistance drops (failure bits) are indicated in symbols. The LRS value is reported as a

dashed line. Panel (c) reports the percentage of devices undergoing fast resistance drop for undoped (blue squares) and doped (red circles) devices after 10^6 s.

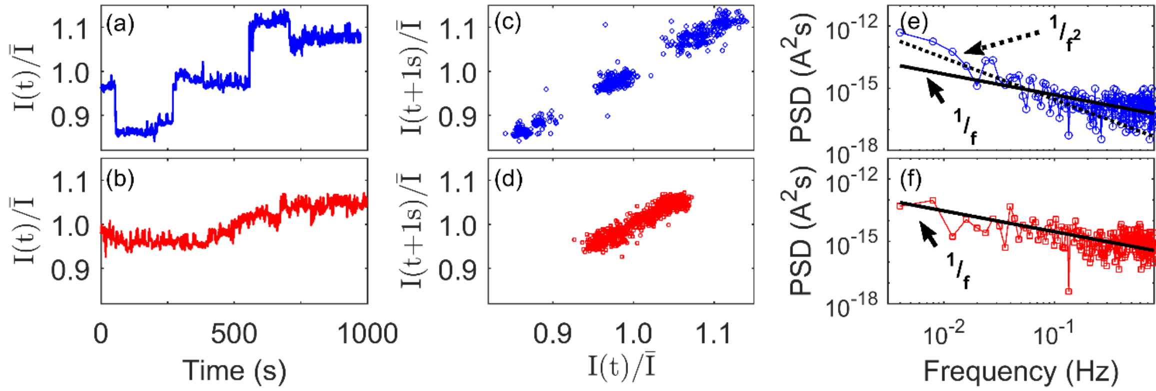

Figure 3. HRS random telegraph noise characterization of both device typologies: (a-b) representative current evolution normalized to the average value over time with time resolution of 1 s; (c-d) representative time 1 s-lag plots and (e-f) power spectral densities.

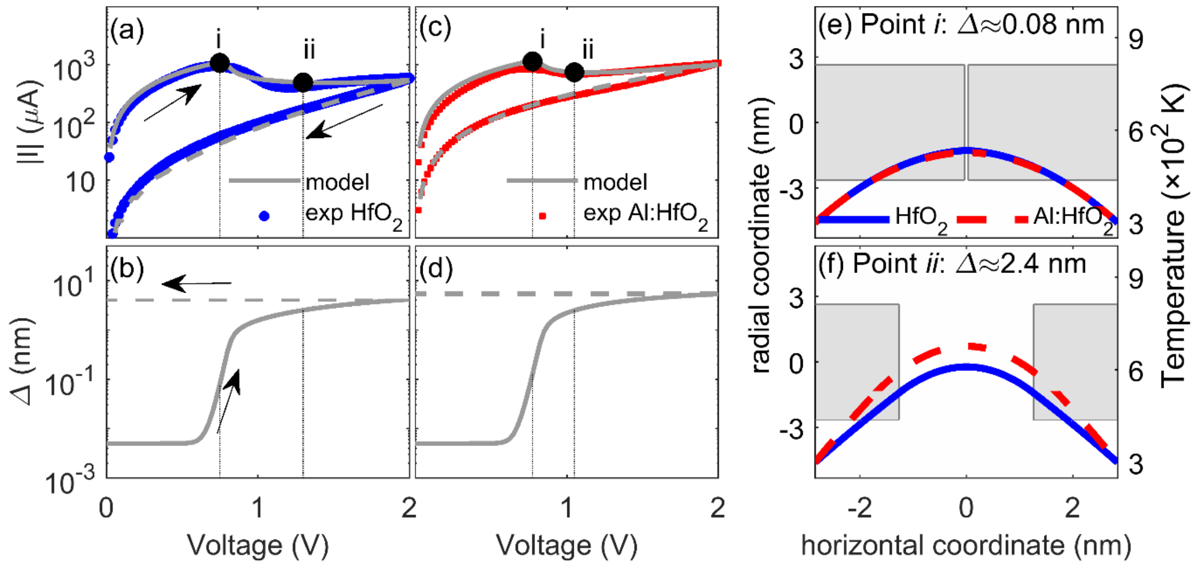

Figure 4. Simulation of the RESET process: (a), (c) average experimental (symbols) and simulated I-V curves (lines) for undoped and doped devices; (b), (d) simulated evolution of the CF gap, Δ, as a function of the voltage for undoped and doped devices. (e), (f) filament configurations (left axis) for Δ ≈ 0.08, 2.4 nm for both undoped and doped devices at points *i* and *ii*, respectively. In the same panels, (right axis) the temperature profiles along the CF axis are shown as (blue) straight and (red) dashed lines for undoped and Al doped devices, respectively.

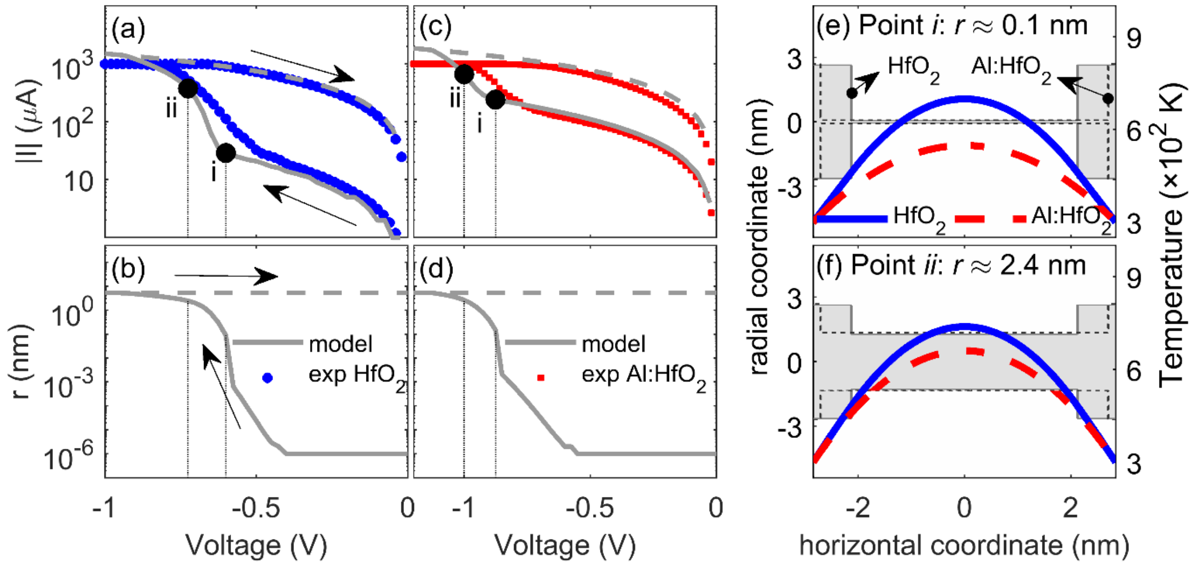

Figure 5. Simulation of the SET process: (a), (c) average experimental (symbols) and simulated I-V curves (lines) for undoped and doped devices; (b), (d) simulated evolution of the CF radius as a function of the voltage for undoped and doped devices. (e), (f) filament configurations (left axis) for $r \approx 0.1$, 2.4 nm for undoped (continuous border line) and doped devices (dashed border line) at points *i* and *ii*, respectively. In the same panels, (right axis) the temperature profiles along the CF axis are shown as (blue) straight and (red) dashed lines for undoped and Al doped devices, respectively.

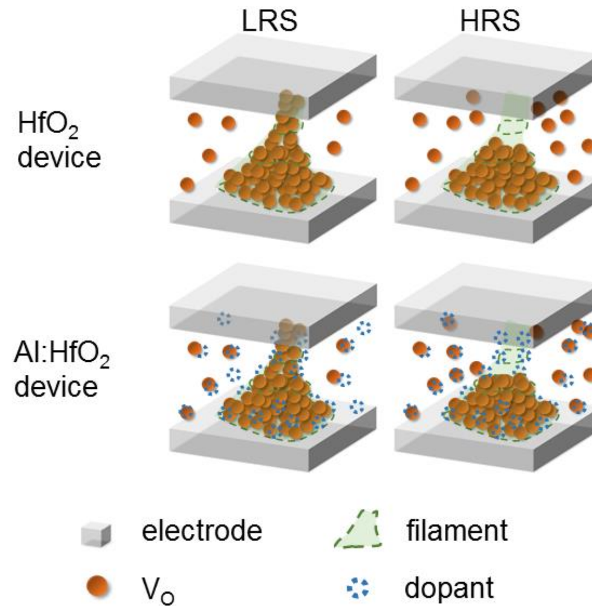

Figure 6. Sketch of filament configurations in LRS and HRS for undoped and Al-doped HfO_2 devices.